Quantitative analysis of the aluminate interactions in model and real cement slag pastes at an early age

Zhang, Yu; Liu, Chaoyu; de Lima Junior, Luiz Miranda; Liu, Chen

DOI
10.1016/j.cscm.2025.e05509

Publication date
2025

Document Version
Final published version

Published in
Case Studies in Construction Materials

Citation (APA)
Zhang, Y., Liu, C., de Lima Junior, L. M., & Liu, C. (2025). Quantitative analysis of the aluminate interactions in model and real cement slag pastes at an early age. *Case Studies in Construction Materials*, *23*, Article e05509. https://doi.org/10.1016/j.cscm.2025.e05509

Case Studies in Construction Materials 23 (2025) e05509

Contents lists available at ScienceDirect

Case Studies in Construction Materials

journal homepage: www.elsevier.com/locate/cscm

Quantitative analysis of the aluminate interactions in model and real cement slag pastes at an early age

Yu Zhang [a], Chaoyu Liu [a], Luiz Miranda de Lima Junior [b], Chen Liu [b,*]

[a] Key Laboratory of Concrete and Prestressed Concrete Structures of the Ministry of Education, Southeast University, Nanjing 210096, China
[b] Microlab, Section of Materials and Environment, Faculty of Civil Engineering and Geosciences, Delft University of Technology, Delft, the Netherlands

ARTICLE INFO

Keywords:
Aluminate peak
Synthetic blast furnace slag
C_3A
Gypsum
Thermodynamic modelling

ABSTRACT

The present research investigated the hydration characteristics of model (C_3S-C_3A-gypsum-blast furnace slag) and real cement slag pastes at an early age, and emphasis was laid on the interaction of gypsum, aluminate phases dissolved from both C_3A and slag. Two additional peaks arose during the decelerating stage of calorimetric measurement. The first one was originated from the renewed aluminate reaction between C_3A and gypsum, while the second one was attributed to the reaction between aluminate phase dissolved from slag and gypsum. High alumina content in slag promoted the aluminate reactions between gypsum and C_3A. On the other hand, the reaction between slag and gypsum was suppressed because of the addition of C_3A. Besides, factors affecting the optimal sulfate requirement of cement slag paste, e.g., C_3A content in cement clinker, slag substitution level, and slag chemistry, etc. were analyzed. The authors believed that the results found in this paper provided essential insights to quantitatively understand the early-age aluminate interactions of gypsum, C_3A as well as blast furnace slag in cement slag paste.

1. Introduction

For cement and concrete production, further increasing the substitution level of cement clinker with supplementary cementitious materials (SCMs) has been considered a practical and effective strategy [1,2]. A wide range of natural and waste resources can be adopted as SCMs, including calcined clays, natural pozzolans from certain geographical sites, blast furnace slag as the by-product of steel manufacturing, fly ash from coal power plants, etc [3–6].

These SCMs contain amorphous phase mainly composed of (calcium) aluminosilicate [6]. Especially, the alumina content varies considerably among different types of SCMs. In consequence, it requires a deeper understanding of sulfate requirement for blended or composite cements, instead of employing the same gypsum addition of Ordinary Portland cement. The work of Durdziński et al. observed a rapidly uncontrolled reaction between aluminate species and gypsum in cement blended with Al_2O_3-rich aluminosilicate glass [7]. On the other hand, it was realized that optimizing gypsum content in cement-calcined clay-limestone ternary blend can increase compressive strength by more than 50 % at one day [8]. These results highlighted the importance of incorporating aluminate phase dissolved from SCMs to calculate the required gypsum content. However, these studies failed to distinguish reactions between gypsum and aluminate phases dissolved from C_3A ($3CaO{\cdot}Al_2O_3$) as well as SCMs, separately.

Among these SCMs, blast furnace slag (*slag* for short) is an end product from iron production. The iron ore gangues, reduced

* Corresponding author.
E-mail address: c.liu-12@tudelft.nl (C. Liu).

https://doi.org/10.1016/j.cscm.2025.e05509
Received 18 August 2025; Received in revised form 7 October 2025; Accepted 1 November 2025
Available online 7 November 2025

substances, and components of melted coke are mixed in the blast furnace to form liquid slag at a temperature of around 1450 °C [9]. Its major constituents, calcium oxide and silica, are present in large quantities. Also, slag consists of significant amounts of minor components, i.e., alumina and magnesium oxide. Thus, it is commonly described as a $CaO\text{-}SiO_2\text{-}Al_2O_3\text{-}MgO$ quaternary system [10]. Depending on the compositions of raw materials fed into the furnace, slag chemistry varies notably across different regions [11,12]. For example, the alumina content of slag produced in Europe varies from 5 to 18 wt% [13]. It is in the range of 7–18 wt% in North America [12,14]. This value fluctuates at 12–15 wt% for slag generated in Austria [15]. As a result, it complicates the sulfate requirement of blended cements, especially at a high slag replacement level (CEM III/B, CEM III/C, etc.) [16].

Therefore, several researchers studied synthetic $CaO\text{-}SiO_2\text{-}Al_2O_3\text{-}MgO$ based glasses with controlled chemical composition in the laboratory conditions [17,18] to simulate commercial slag encountered in market. This approach was particularly preferred in order to eliminate potential interferences from other internal or external sources. These studies showed that chemical composition played a key role on the slag network structure, which affects the surface free energy, hence its reactivity. It was generally recognized that the reactivity increases with increasing depolymerization of the silicate structure. However, these studies did not go further to investigate the interaction among cement clinker, gypsum, and blast furnace slag-like glass in the real blended systems.

In our previous work, the authors studied the hydration characteristics of C_3S ($3CaO{\cdot}SiO_2$, the major constituent of cement clinker), gypsum, and synthetic blast furnace slag system at an early age (before 3 days), without C_3A ($3CaO{\cdot}Al_2O_3$, the most reactive constituent of cement clinker) addition [19]. It was found that the reaction rate of aluminate reaction was governed by the availability of different reactants. Calcium monosulfoaluminate (*monosulfate* for short) only occurred in Al_2O_3-rich slag mixture. With this simplified model paste (It is well recognized that the other two constituents, C_2S and C_4AF, contribute little at early age due to their relatively less reactive property.), the contribution to aluminate peak sourced from aluminate phase in blast furnace slag was identified. However, in the presence of slag, the interaction of aluminate phases dissolved from C_3A and slag complicates the hydration mechanism of blended cement at an early age.

Therefore, this paper attempted to answer this question, using blast furnace slag-like glass to simulate commercial slag. In the study, analytical C_3A reagent was introduced into the model mixture, and emphasis was laid on the interaction among gypsum, aluminate species released from C_3A and blast furnace slag-like glass at an early age. To highlight the interaction between gypsum and aluminate phases dissolved from slag, model pastes containing 30 wt% $C_3S + C_3A +$ gypsum and 70 wt% blast furnace slag-like glass with different Al_2O_3 contents were utilized to simulate CEM III/B. Moreover, real cement-synthetic blast furnace slag paste was also cast as a reference. The authors believed that the results found in this paper provided essential insights to quantitatively understand the early interaction of gypsum, C_3A as well as blast furnace slag.

2. Materials and methodology

2.1. Materials

Three synthetic blast furnace slags (A3, A12, and A18) with different Al_2O_3 contents were produced in the laboratory and adopted for specimen casting in the present study. The synthetic slag was prepared by mixing a commercial slag and AR (analytical reagent) CaO, MgO, SiO_2, Al_2O_3 according to different compositional design targets. Details of the synthesis process are given elsewhere [19]. Analytical grade reagent C_3S, C_3A, and gypsum (provided by Merck, Germany) were employed to prepare $C_3S\text{-}C_3A$-gypsum-synthetic

Table 1
Chemical compositions (wt%) determined by XRF analysis and physical properties of the raw materials.

	Cement	A3	A12	A18
CaO	64	42.07	37.32	36.87
SiO_2	20	43.30	39.11	34.43
Al_2O_3	5	**3.69**	**12.32**	**18.19**
MgO	-	10.83	9.43	7.98
Fe_2O_3	3	0.07	0.30	0.40
TiO_2	-	-	0.70	0.84
MnO	-	-	0.15	0.27
Na_2O	-	-	0.24	0.37
K_2O	-	-	0.21	0.41
SO_3	2.93	0.01	0.03	0.03
Others	5.07	0.03	0.19	0.21
LOI[a]	-	−0.02	−0.03	−0.04
Physical properties				
D_{10} (μm)[b]	5.83	3.93	5.27	4.77
D_{50} (μm)	26.81	19.67	20.35	20.85
D_{90} (μm)	63.38	42.83	41.41	36.93
SSA (m^2/g)[c]	0.284	1.09	0.919	0.904

[a] . The loss-on-ignition (LOI) value of synthetic slag was determined by thermogravimetric analysis at 950 ± 50 °C. The negative value of LOI was related to the oxidation of sulfur rich species in slag. It should be noted that the LOI value was not corrected in the XRF measurement.

[b] . The particle size distribution (PSD) of CEM I 42,5 N and synthetic slag was measured by EyeTech, Ankersmid. The d_{50} of quartz was 24.21 μm.

[c] . The specific surface area (SSA) of CEM I 42,5 N and synthetic slag was measured by Blaine and nitrogen adsorption with the BET methods, respectively.

slag (or quartz) system, as model paste. On the other hand, CEM I 42,5 N (manufactured by ENCI B.V., Netherland) was also adopted to generate real cement-synthetic slag (or quartz) paste.

The chemical compositions determined by X-ray fluorescence (XRF) spectrometer and physical properties of raw materials are exhibited in Table 1. The CaO/SiO_2 mass ratios of three slags were kept at around 1.0 and the amounts of MgO were stabilized at about 9.0 wt%. On the other hand, alumina content increased from 3.69 (A3) to 18.19 wt% (A18). Note that trace of Fe_2O_3, TiO_2, and MnO were observed in these slags, and it was inevitable due to the adoption of commercial slag as raw material for production. Three slags and quartz presented a similar particle size distribution, with a $d_{50} \approx 20.0$ μm.

A representative X-ray diffraction (XRD) result of C_3S is shown in Fig. 1(a), and the result indicated that it exhibited a triclinic polymorph. For another, when compared to the XRD patterns of cubic C_3A (ICDD PDF No. 38–1429) and the orthorhombic one (ICDD PDF No. 26–0958), it can be found that the C_3A adopted in this paper was primarily cubic (Fig. 1(b)). Besides, the C_3A employed here was relatively coarse, with a $d_{50} \approx 13.2$ μm, coarser than those which typically exhibited a d_{50} of several micron [20,21]. As for synthetic slag, they were entirely amorphous with no obvious crystal peak [22].

The ^{29}Si and ^{27}Al MAS NMR spectra of synthetic slag is given in Fig. 2. The ^{27}Al spectra presented a broad resonance in the region between 50 and 80 ppm with a center of gravity at approximately 60 ppm, assigned to tetrahedral Al environment. This peak can be attributed to the amorphous phase composing the majority of slag, consistent with the hump identified by XRD scan in Fig. 1. Results in [23] also elucidated that for higher calcium content (Ca/Al > 1), Al was almost solely present in four-fold coordination, and the contribution from five- and six-fold coordination was very low. The obtained ^{29}Si spectra exhibited a broad peak between −60 and −90 ppm centered at around −75 ppm, covering the range of chemical shift from Q^0 to Q^3 unit of Si tetrahedra. It confirmed that most CaO available in slag acted as non-bridging oxygen generator. Nearly no impact on both ^{29}Si and ^{27}Al spectras can be observed when the mass percentage of Al_2O_3 in slag rose from 3.69 to 18.19 wt%. It demonstrated that the gradual incorporation of Al into silicate tetrahedra did not affect the atomic environment of aluminum and the existence of Q^n specie [23].

2.2. Mix design and experimental methods

Mix design of model paste prepared for each group is reported in the following Table 2. The synthetic slag including A3, A12, and A18 (or quartz) to $C_3S + C_3A +$ gypsum ratio was kept at 7/3 and water to binder ratio was 0.40. C_3A and gypsum were introduced to replace C_3S, and the C_3S to C_3A ratio was maintained at 7.6 throughout the research, to keep identical with that of CEM I 42,5 N. Each group was named as the corresponding sulfate content with respect to $C_3S + C_3A +$ gypsum, i.e., G3, G5, and G10 for sulfate dosage level of 3, 5, and 10 %, respectively. Compared to the C_3S-gypsum-slag mixture, G0 and G1 representing sulfate dosage level of 0 and 1 % were not considered here to avoid an undersulfated system [19]. As for the nomenclature of each specimen, using G3_A18 as an example, it indicated that 3 % sulfate dosage and synthetic slag A18 were employed.

Additionally, 70 wt% cement was replaced by synthetic slag (or quartz) to produce binary cement-slag (or quartz) system simulating CEM III/B, with a same water/binder ratio of 0.40.

Heat evolution of the paste was observed using a TAM Air isothermal calorimeter at 20 °C over the course of three days. Raw materials were mixed at a high speed for 2 min, and approx. 7 g of the mixture was placed in a glass ampoule and transported to the calorimeter to be evaluated (For calorimetric measurements, they were stopped at 4 days, and the corresponding results were given in the paper.). Paste specimens mounted in plastic bottles of 20 mL were prepared in the same manner. All the specimens were kept sealed at ambient temperature for 3 days before any measurements.

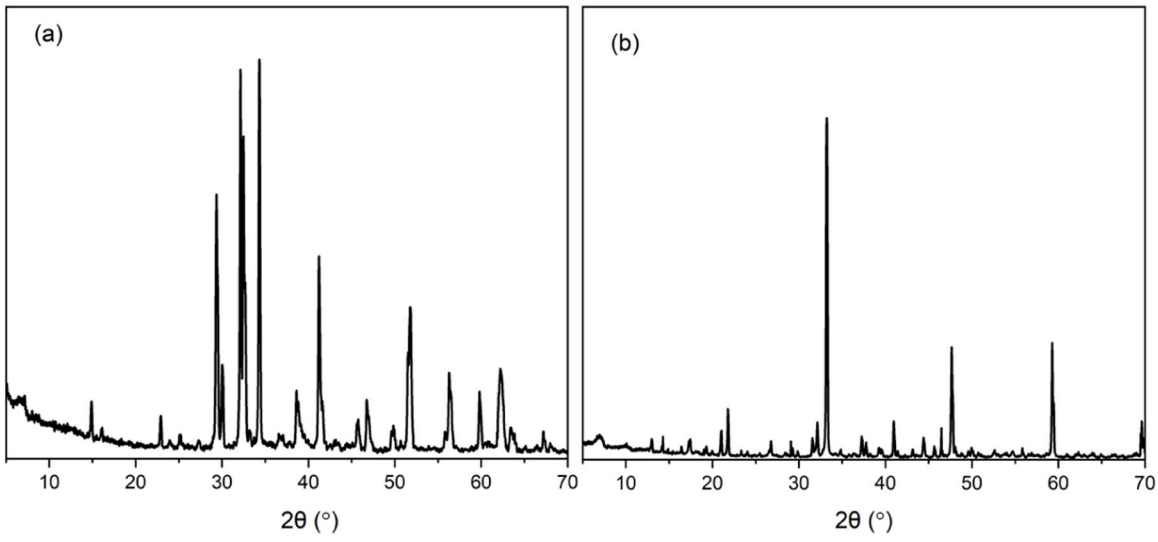

Fig. 1. X-ray diffractogram of (a) C_3S and (b) C_3A.

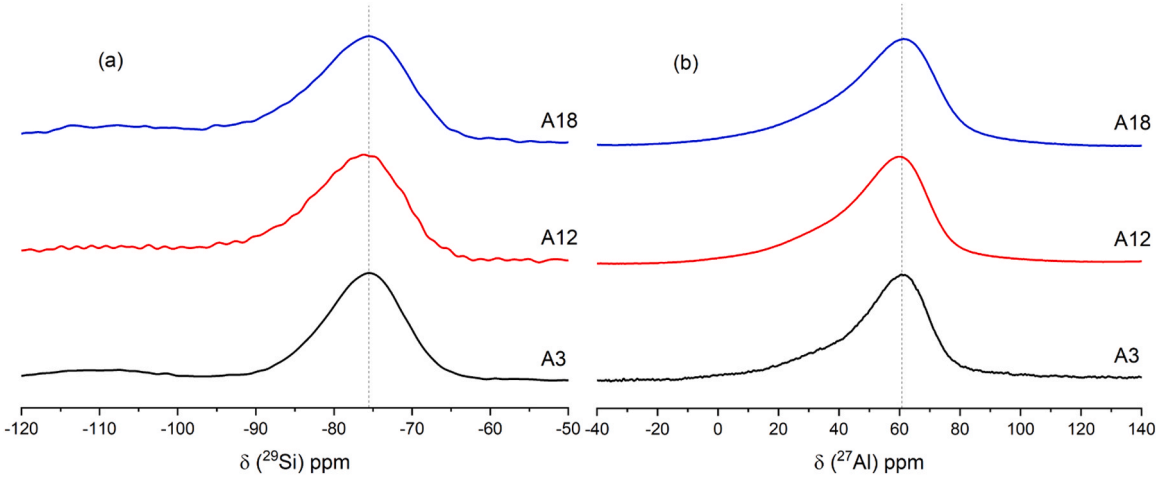

Fig. 2. (a) ^{29}Si and (b) ^{27}Al MAS NMR spectra of synthetic slag.

Table 2
Composition (wt%) of each paste.

	C_3S	C_3A	gypsum	slag	C_3S/C_3A	$SO_3/(C_3S+C_3A+gypsum)$	slag/(C_3S+C_3A+gypsum)
G3	24.805	3.260	1.935	70	7.6	3 %	7/3
G5	23.665	3.110	3.225	70	7.6	5 %	7/3
G10	20.815	2.735	6.450	70	7.6	10 %	7/3
	cement			slag			slag/cement
	30			70			7/3

After 3 days of curing, specimens were crushed, and the selected slices were placed in isopropanol solution to extract free water. These slices were further ground and sieved manually to obtain fine powder (< 63 μm). Netzsch STA 449 F3 Jupiter was used for thermogravimetric analysis (TGA). Approx. 50 mg sample powder was heated up from 40 to 800 °C (10 °C per min) under an argon atmosphere. As for XRD scan, a Philips Powder Diffractometer PW 1830/40 with Cu K-alpha radiation was employed to collect data. Powder was scanned from 5 to 40° (2θ) at an acceleration voltage of 40 kV and an X-ray beam current of 40 mA, with a step size of 0.03°.

Solid state magic angle spinning (MAS) nuclear magnetic resonance (NMR) measurement was performed on Bruker Ascend 500 Magnet (11.7 T) equipped with a NEO console operating at ^{29}Si and ^{27}Al resonance frequencies of 130.32 and 99.36 MHz respectively, using both 4 and 3.2 mm three channel MAS probe heads to check the atomic environment of Si and Al. Powder sample, ground to a fineness below 63 μm was used in the test. The MAS rate was set up between 10 and 15 for all measurements. Single pulse one-dimensional (1D) measurement was recorded for ^{29}Si and ^{27}Al with pulse lengths of 1.5 μs and 3.5 μs corresponding to 30° and 90°

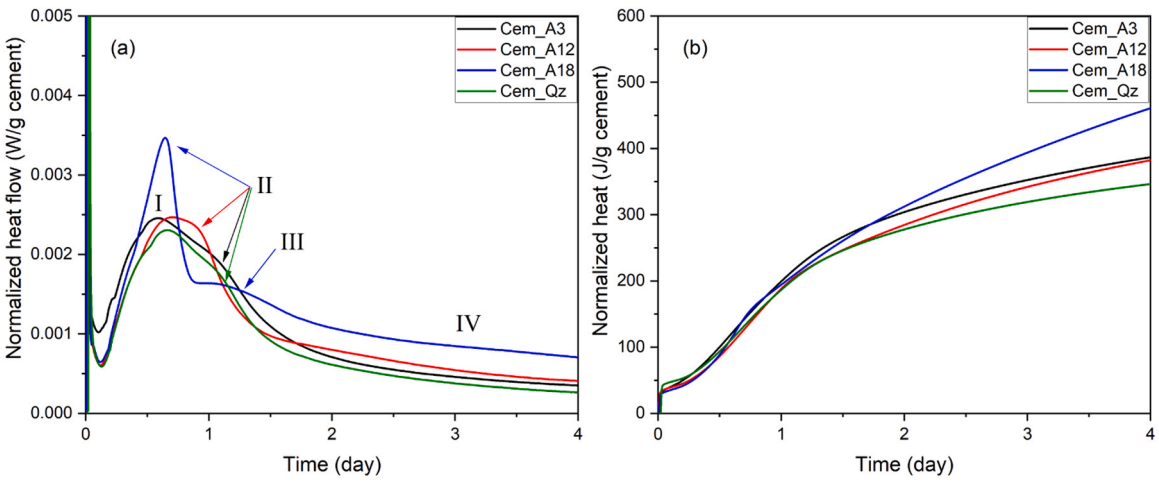

Fig. 3. Calorimetric curves of cement-slag (or quartz) systems. (a) normalized heat flow; (b) cumulative heat release.

pulses, respectively. Recycle delays of 30 s for ^{29}Si and 3 s for ^{27}Al were set up to allow for complete recovery of magnetization between scans.

With some fractural surfaces, the morphology of typical hydrates was observed in a secondary electron (SE) mode with an FEI QUANTA FEG 650 ESEM, operated at a working distance of 10 mm and an accelerating voltage of 15 kV.

Thermodynamic modelling was also performed using the Gibbs free energy minimization software GEM-Selektor (GEMS) with thermodynamic data from the PSI-GEMS database supplemented by cement specific data [24–26]. For simplicity, some assumptions were introduced. For example, it was assumed that reactants hydrated to different hydration degrees, and slag dissolved congruently (especially for fine slag grains).

3. Results

3.1. General hydration pattern of real cement-slag system

Fig. 3(a) displays the heat evolution rate of cement-slag (or quartz) system, normalized to per gram of cement. The cement-quartz mixture was dominated by one main peak (labelled as peak I) within 24 h, related to the hydration of C_3S in cement clinker, and followed by a shoulder/aluminate peak (peak II), which suggested the secondary aluminate reaction between C_3A and gypsum (~12 h after the main peak). With the increasing Al_2O_3 content in slag, the onset of peak II became earlier. In A18 slag blend, it even superimposed the main hydration peak I, leading to an intensified sharp peak. Aluminate peak in cement-slag system involved the reactions between gypsum and aluminate phases dissolved from C_3A as well as slag together. Considering that synthetic slag and quartz presented a similar particle size distribution and specific surface area, the difference regarding aluminate peak can be attributed to slag chemistry, i.e., the Al_2O_3 content. Aluminate phase dissolved from slag reacted with sulfate from gypsum for the formation of ettringite and thus contributed to the aluminate peak. However, it was not possible to quantitatively distinguish the contributions of C_3A and slag separately due to the overlap.

After one day, a third hydration peak (peak III), or hump, can be observed (especially for slag A18 blend). Slag started to react with $Ca(OH)_2$, and this pozzolanic reaction (The chemical reaction between the siliceous-alumina components in the slag, calcium hydroxide, and water is called as pozzolanic reaction.) contributed to this hump. Finally, a continuous and steady hump (peak IV) characterizing the transformation from ettringite to monosulfate was also seen in all systems.

Fig. 3(b) displays the cumulative heat release, normalized to per gram of cement. Before one day, all curves were almost identical, proving that slag acted as an inert filler like quartz and only provided extra site. The reaction degree of cement clinker in all mixtures was similar. However, curves deviated from each other from then on. Aluminate species dissolved from slag participated into the formation of ettringite and contributed to the aluminate peak [27,28]. Also, fine slag particles reacted with $Ca(OH)_2$ (Note that slag A3 exhibited the fineness particle size distribution.). These reasons explained that Al_2O_3-rich slag A18 blend evolved the most heat while a lower cumulative heat release was seen in Cem_A12 paste, as a result.

The incorporation of slag with different alumina contents affected the aluminate peak significantly, including onset timing, intensity, etc. However, it was not possible to quantitatively distinguish the contributions of C_3A and slag separately based on cement-slag system. Thus, C_3S-C_3A-gypsum-slag system was prepared in the study and analyzed in the following sections. Combining the results of C_3S-gypsum-slag pastes, the authors attempted to quantitatively determine the influence of C_3A and blast furnace slag on the hydration rate and degree of each other, as well as the optimal gypsum content involving the contribution of aluminate phase released by slag.

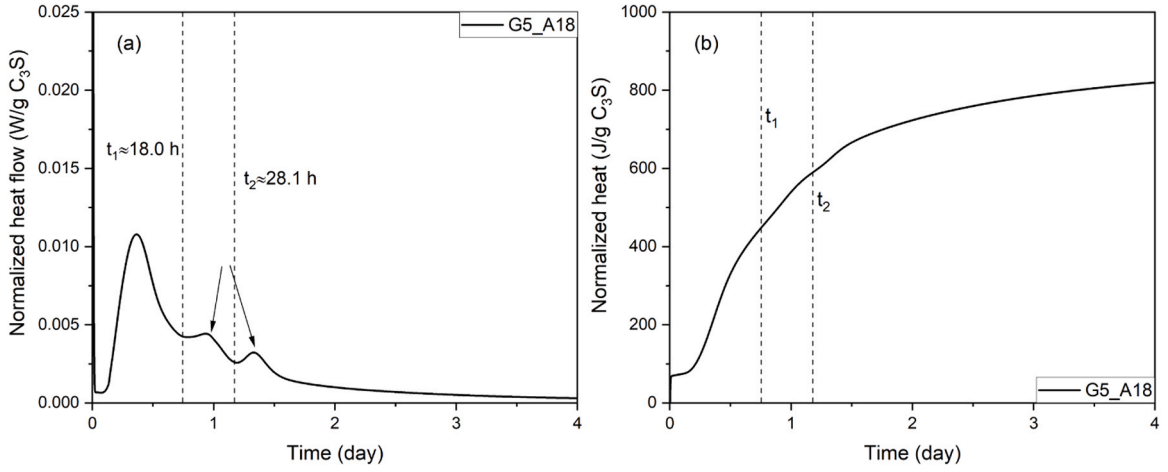

Fig. 4. (a) Heat flow and (b) total heat release as a function of time from calorimetric measurement for C_3S-C_3A-5 % SO_3-slag A18 system.

3.2. General hydration pattern of C_3S-C_3A-gypsum-slag system

Fig. 4(a) and (b) illustrate the heat flow and total heat release of C_3S-C_3A-5 % SO_3-slag A18 system (*G5_A18* for short, and the same naming method was applied below.), normalized to per gram of C_3S correspondingly. The heat evolution rate was dominated by the main hydration peak, originated from the hydration of C_3S (Fig. 4(a)) [21]. After the main peak, two additional peaks were visible, which were related to the aluminate reactions between sulfate and aluminate species dissolved from C_3A as well as slag, respectively. For the first one, it initiated at ~18.0 h (t_1) upon contacting with water while it was around 28.1 h (t_2) for the second one. In the following parts, the authors would lay emphasis on these two aluminate reactions.

3.2.1. Effect of C_3A addition

Fig. 5(a)-(c) exhibit the heat flow of C_3S-3, 5, and 10 % SO_3-slag A18 systems with and without C_3A addition. The only additional peak observed in blends without C_3A addition (red dashed line in the graphs) represented the reaction between aluminate phase released by slag and sulfate sourced from gypsum, for the precipitation of ettringite [19].

With the introduction of C_3A, another peak was detected in each blend, as indicated by black arrow in the figures. This peak suggested the reaction of aluminate phase from C_3A with sulfate from gypsum as the following equation elucidates, which was consistent with the results of TGA (Fig. 12) and XRD (Fig. 13) in the following part:

$$6Ca^{2+} + 2AlO_2^- + 3SO_4^{2-} + 4OH^- + 30H_2O \rightarrow Ca_6Al_2(SO_4)_3(OH)_{12}\cdot 26H_2O$$

Furthermore, the intensity of main hydration peak of C_3S was found to increase slightly compared to mixtures without C_3A incorporation. It agreed with results that the hydration degree of C_3S in properly sulfated C_3S/C_3A system was higher than pure C_3S system [21]. On the other hand, the hydration rate after 2 days (steady stage) seemed to be unaffected by the existence of C_3A, and the curves (with and without C_3A) overlapped with each other.

3.2.2. Effect of gypsum

As shown in Fig. 6(a), the hydration rate during acceleration and steady period was nearly the same with different gypsum additions. In consequence, the curves of cumulative heat release overlapped completely before one day. However, the results in [29] proved that gypsum retarded the initial hydration (first 3 h) of both C_3S and Al-C_3S due to the interaction between the sulfate ion and C_3S. In contrast, gypsum enhanced their hydration afterward. However, with C_3A introduction which was more reactive than C_3S, the sulfate ion in the pore solution tended to be absorbed on the surface of C_3A. Therefore, more research is needed to clarify it in the future.

On the other hand, the main difference occurred during the deceleration stage (0.5–2 days after mixing). More heat was evolved with increasing gypsum addition (Fig. 6(b)), implying an enhanced aluminate reaction and thus ettringite precipitation. Two additional peaks arose at this period in the mixtures of G5_ and G10_A18, both of which were delayed correspondingly with the progressive incorporation of gypsum. For G3_A18 paste, only one aluminate peak was observed during the deceleration period.

The first additional peak can be associated with the renewed aluminate reaction between C_3A and gypsum, and it was comparable to the shoulder occurred in pure cement system after main hydration peak (Fig. 3(a)). Due to the absorption of sulfate ion on reactive sites of C_3A, its dissolution was inhibited in the first hours. When sulfate ion in the pore solution was consumed by the absorption of C−S−H gel phase or formation of ettringite covering the active surface of C_3A, this peak was initiated [30,31]. It occurred just following the main hydration peak of alite in a properly sulfated Portland cement. Thus, it was no wonder that the onset of this peak was delayed with the gradual gypsum introduction, i.e., it was postponed from about 18.0 h (t_1) to approximately 22.7 h (t_1) for systems with 5 and 10 % sulfate dosage levels.

Following the first aluminate peak, the second one was also delayed (t_2: ~28.3 h → ~32.6 h) and became broader with continuous gypsum incorporation. This peak was regarded to be sourced from the reaction between aluminate species dissolved from slag (less

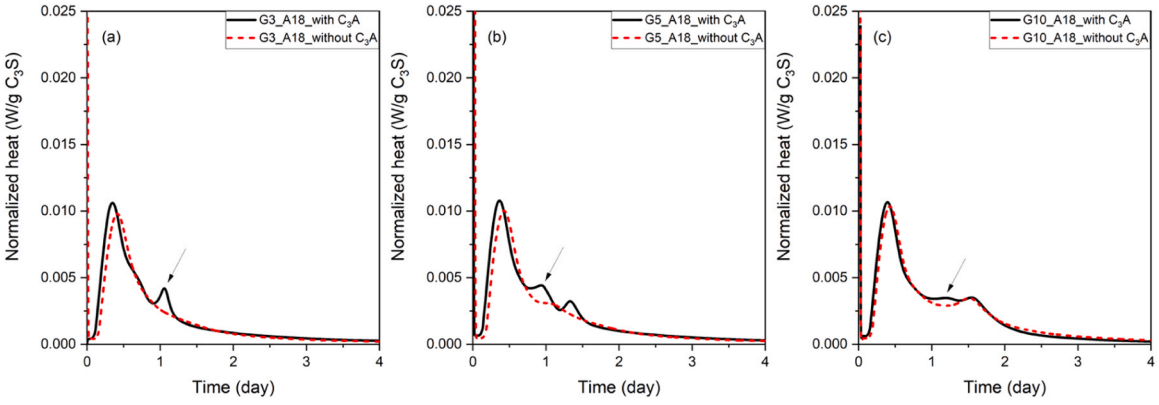

Fig. 5. (a)-(c) Heat flow of C_3S-3, 5, and 10 % SO_3-slag A18 systems with (black solid line) and without (red dash line) C_3A addition.

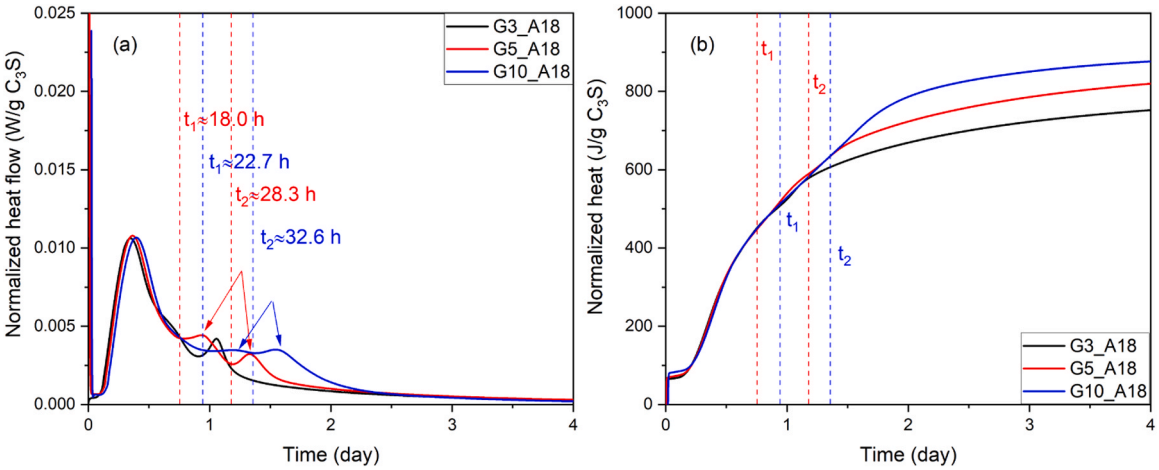

Fig. 6. (a) Heat flow and (b) total heat release as a function of time of C_3S-C_3A-SO_3-slag A18 system with different amounts of gypsum.

reactive compared to C_3A) and sulfate from gypsum. In fact, in terms of factors controlling the occurrence of this peak, possibilities of another two reactions should be analyzed:

(1) Pozzolanic reaction between slag and portlandite

If pozzolanic reaction dominated this peak, a severely eroded slag surface should be observed. However, as demonstrated in Fig. 14 (d)-(f), the majority of slag surface kept intact even after 3 days of curing. Thus, pozzolanic reaction cannot be the controlling mechanism although some early reactions between fine slag grains and portlandite contributed to this peak to some extent, at such a high slag substitution rate.

(2) Transformation from ettringite to monosulfate

In general, the transformation from ettringite to monosulfate was a continuous process and it was unlikely to happen in a short period [32,33]. In addition, if it was the governing reaction of this peak, few ettringite was expected to be seen in the mixture; however, it was opposite to the results illustrated in Fig. 13 (a) and 14 (a)-(c), where ettringite was widely observed in the matrix.

3.2.3. *Effect of Al_2O_3 content in slag*

Fig. 7(a) and (b) present the heat flow and cumulative heat release of C_3S-C_3A-5 % SO_3-slag systems with different Al_2O_3 contents in slag. The hydration of model paste was unaffected by Al_2O_3 before the first 12 h; however, it played a key role during the deceleration period. These two additional peaks were noted distinctly in slag A18 mixture while no evident peak was found in A3 blend. On the other hand, they existed as a broad hump in the system of slag A12. Therefore, it can be concluded that the renewed aluminate reaction between C_3A and gypsum was accelerated because of the high alumina content in slag. As for C_3S-C_3A-5 % SO_3-quartz blend,

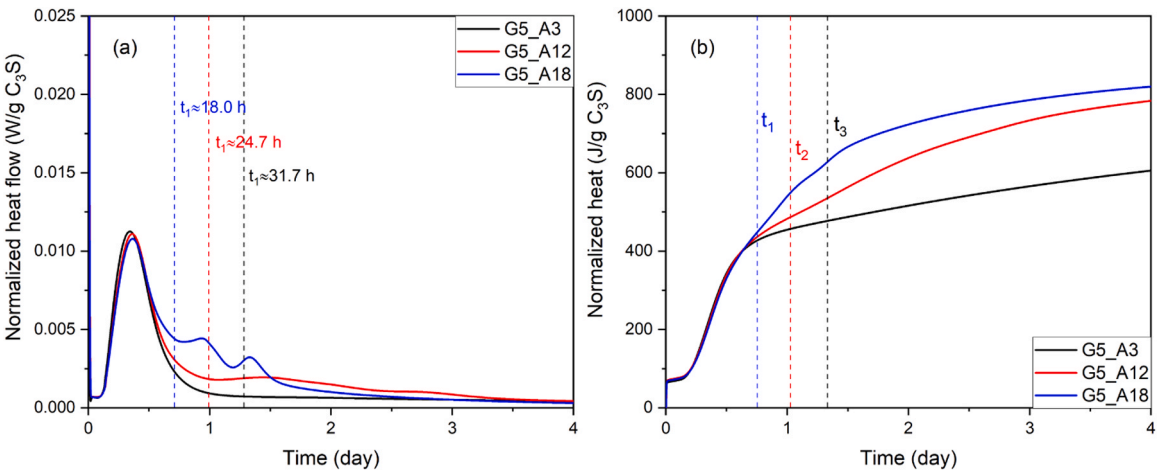

Fig. 7. (a) Heat flow and (b) total heat release as a function of time from calorimetric measurement of C_3S-C_3A-5 % SO_3-slag systems with different Al_2O_3 contents in slag.

the calorimetric result was almost same to slag A3, and cannot be distinguished from the graph. Thus, it was not exhibited here.

As revealed before, the adsorption of sulfate ion on the defect sites inhibited the further hydration of C_3A and explained the formation mechanism of induction period [30,31]. When gypsum was consumed, the depletion of sulfate ion in the pore solution caused a net desorption of sulfate from the surface of C_3A. Following, the reaction between C_3A and gypsum was renewed, and a shoulder was commonly noticed in the heat flow graph, behind the main hydration peak. With the addition of slag, the aluminate phase released by slag promoted the depletion of sulfate ion. Thus, the renewed reaction between C_3A and gypsum was accelerated with increasing alumina content in slag (t_1: ~31.7 h → ~24.7 h → ~18.0 h). It agreed well with the results obtained in [27], all of which noted that slag addition accelerated and enhanced the renewed hydration of C_3A.

Besides, high alumina content in slag also promoted the aluminate reaction between slag and gypsum, as found in [19]. It was reasonable as Al_2O_3-rich slag typically presented a high reactivity [22,34,35]. Therefore, it can be summarized here that the more Al_2O_3 in slag, the earlier onset of renewed C_3A hydration, the enhanced aluminate reactions between sulfate and aluminate species dissolved from both C_3A and slag, and thus the more heat released (Fig. 7(b)). The cumulative heat release curves overlapped up to ~12 h, and they deviated with each other from then on.

3.2.4. *Heat release from two aluminate reactions*

In this section, the authors attempted to decouple these two aluminate reactions based on calorimetric measurement as much as possible and quantitatively determine the heat evolved from each of them. The calorimetric results of C_3S-5 % SO_3-slag A18 and C_3S-C_3A-5 % SO_3-slag A18 systems were employed as examples to illustrate the calculation process, which was reported in Fig. 8(a) and (b). Total heat evolution of C_3S-5 % SO_3-quartz mixture was also plotted as a reference.

For C_3S-C_3A-5 % SO_3-slag A18 mixture, the first aluminate peak, implied the reaction between C_3A and gypsum occurred at ~18.0 h (t_1) upon contacting with water. It was around 28.1 h (t_2) for the second one, indicated the reaction between slag and gypsum, up to ~38.4 h (t_{end}). As for C_3S-5 % SO_3-slag A18 blend, the only aluminate peak initiated at approximately 21.5 h, and it ended at a similar timing, i.e., $t_{end} \approx 38.4$ h. The corresponding heat emitted at each specific time range was indicated in Fig. 8(b). It should be emphasized that the heat released by C_3S-5 % SO_3-quartz mixture was adopted as baseline for calibration.

Fig. 9 displays the amount of heat released from different aluminate reactions of C_3S-(C_3A)-SO_3-slag A18 systems at various sulfate dosage levels. When without C_3A addition, a positive correlation between sulfate content and heat release of aluminate reaction between slag and gypsum was noticed (*purple columns*). As explained in [19], aluminate phase was adequate in this case, and the availability of sulfate dominated. However, this reaction was suppressed due to the hydration of C_3A, as confirmed by the reduced heat evolution from the second aluminate reaction (*green columns*). This phenomenon can be explained by the common ion effect where aluminate phase dissolved from C_3A suppressed the dissolution of slag (adsorption of AlO_2^- on slag surface) and vice versa. Additionally, it was found that the heat originated from the first aluminate reaction increased with enhanced gypsum addition (*yellow columns*), although the increment was limited when sulfate content was greater than 5 %, and it was overtaken by the second aluminate reaction (*green columns*) at 10 % sulfate dosage level. Considering high slag substitution (70 wt% in the mixture) and alumina-rich slag (18.19 wt% for slag A18), more aluminate phases can be dissolved, participate into the formation of ettringite, and thus more heat was released by the second aluminate reaction at high gypsum dosage.

Considering the formation enthalpy ($\Delta_f H^0$) of ettringite [25], the corresponding hydration degrees of C_3A and slag in C_3S-(C_3A)-SO_3-slag A18/quartz systems at various sulfate dosage levels were thus calculated and given in Fig. 10 (For the detailed calculation method, the readers can refer to [21].). For one thing, the introduction of C_3A hindered the hydration of slag, irrespective of sulfate dosage level. For another, the gradual incorporation of gypsum boosted the hydration of C_3A, and its reaction degree reached 80 % at 10 % sulfate content. Slag addition also enhanced C_3A hydration when compared to C_3S-C_3A-SO_3-quartz blend. As mentioned,

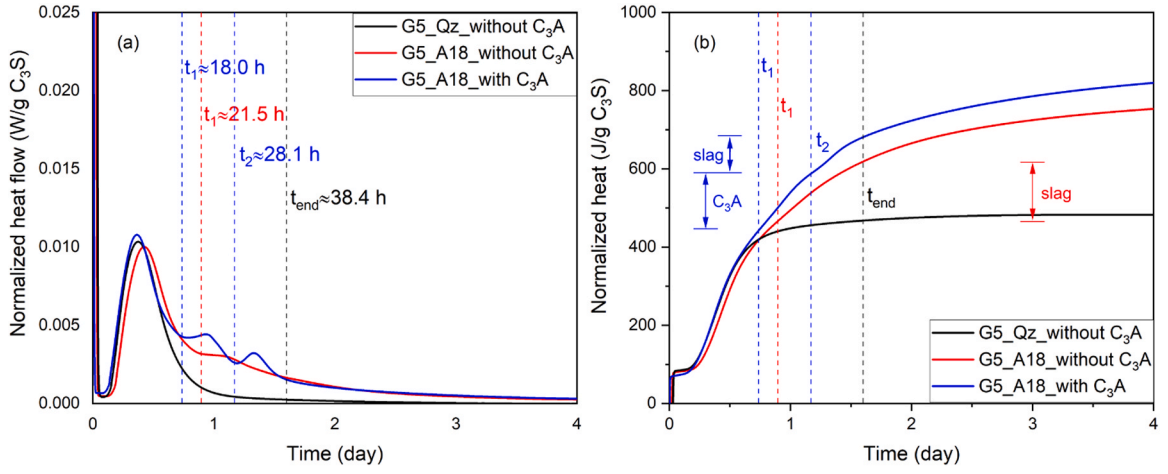

Fig. 8. (a) Heat flow and (b) total heat release as a function of time from calorimetric measurement of C_3S-5 % SO_3-slag A18, C_3S-C_3A-5 % SO_3-slag A18, and C_3S-5 % SO_3-quartz systems.

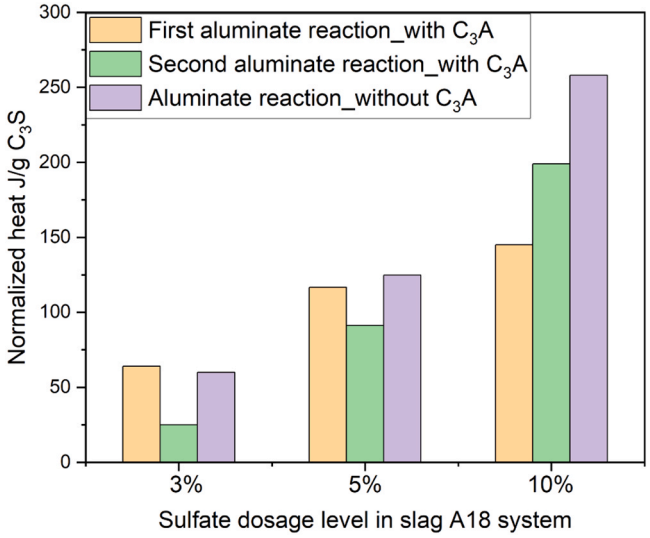

Fig. 9. Heat released from different aluminate reactions of C_3S-(C_3A)-SO_3-slag A18 systems vs. various sulfate dosage levels.

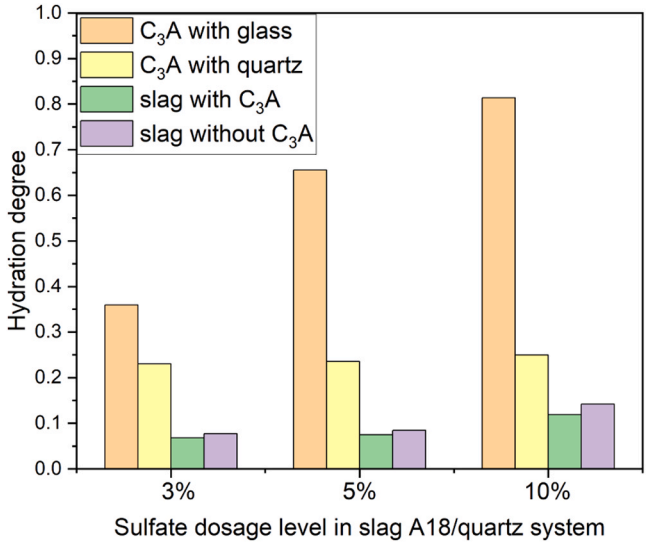

Fig. 10. Hydration degrees of C_3A and slag in C_3S-(C_3A)-SO_3-slag A18/quartz systems vs. various sulfate dosage levels.

the aluminate species dissolved from slag promoted the depletion of sulfate ion in the pore solution. Thus, the renewed reaction between C_3A and gypsum was accelerated in Al_2O_3-rich slag paste. Interestingly, when without the synergistic effect of slag, the positive influence on C_3A hydration exerted by gypsum was marginal (see the yellow column).

Meanwhile, C_3A started to hydrate upon wetting, until the onset of dormant stage [21]. This process was not considered in this paper when determining the hydration degree of C_3A. However, the C_3A adopted in the present study was relatively coarse, and its hydration degree was only slightly higher than 20 % in C_3S-C_3A-SO_3-quartz systems. It indirectly confirmed that the reaction between C_3A and gypsum at the first minutes upon mixing with water was negligible. On the other hand, one should keep in mind that the results reported in Fig. 10 can only be considered approximately, as the formation of ettringite/monosulfate was overlapped after the main hydration peak, and the enthalpy associated with the formation of ettringite from C_3A and slag was different.

In C_3S-C_3A-SO_3-slag A3 and A12 blends, these two aluminate reactions cannot be distinguished clearly owing to the overlap. Thus, they were considered as a whole, and the results were reported in the following Fig. 11.

For C_3S-(C_3A)-SO_3-slag A3 pastes, a slight increase was seen for the heat evolved from these two aluminate reactions. Under this circumstance, it was convincible to conclude that the amount of gypsum added was adequate, and the availability of aluminate phase was the rate-controlling factor. The gap for slag A3 mixtures with and without C_3A introduction at the same sulfate content can be assigned to the heat released by the hydration of C_3A, approximately. Slag with a low alumina content presented a similar role to

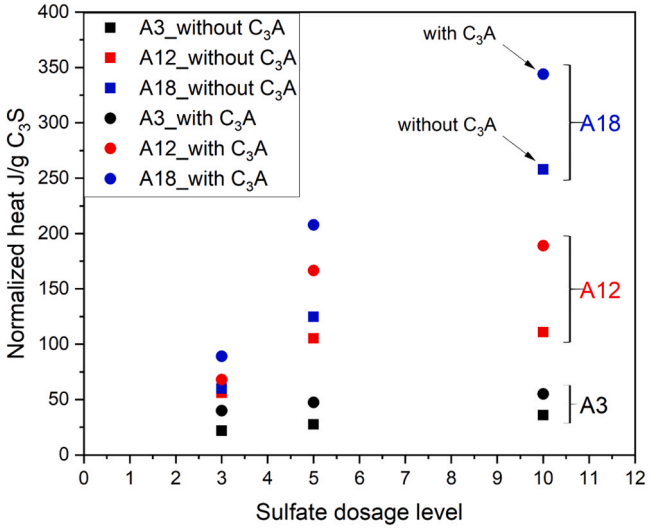

Fig. 11. Heat released from two aluminate reactions of C_3S-(C_3A)-SO_3-slag systems vs. various sulfate dosage levels.

quartz, and the C_3A hydration cannot be boosted with gypsum solely.

For slag A12 mixtures, the heat released from two aluminate reactions went up notably when the sulfate content increased from 3 % to 5 %; however, it seemed to level off with continuous gypsum addition to sulfate dosage level of 10 %, for both blends. Therefore, when the sulfate content was less than 5 %, there was abundant aluminate phase in the pore solution to participate into the reaction, and the availability of SO_4^{2-} ion was the rate-controlling factor. With increasing gypsum incorporation, the aluminate species dissolved from C_3A and/or slag was consumed and the availability of AlO_2^- ion became the governing parameter. Moreover, the synergistic effect of slag and gypsum on accelerating C_3A hydration became evident at this alumina level of slag.

As for slag A18 blends, a significant increase for heat evolution was found, with the rising of gypsum introduction. In this case, aluminate phase was adequate, and the availability of sulfate dominated. Table 3 summarizes the rate-controlling factor of aluminate reaction in each run of C_3S-C_3A-SO_3-slag systems.

3.3. Hydration products

DTG results of typical C_3S-C_3A-gypsum-slag mixtures at 3 days are exhibited in Fig. 12 (a). Corresponding to the main hydration peak observed in calorimetry measurement (Figs. 3–8 in Sections 3.1 and 3.2), the peak between 400 and 500 °C was indicative of the dehydration of portlandite. As for the mass loss from 100 to 150 °C, it was originated from the decomposition of C−S−H gel phase and ettringite, which cannot be deconvoluted because of the overlap. A minor amount of hydrotalcite-like phase (mass loss at around 350 °C) was also identified. In addition, monosulfate (mass loss at around 200 °C) was found to precipitate in slag A12 and A18 blends after 3 days of curing.

The DTG results of cement-slag groups are shown in Fig. 12 (b). Consistent with the results obtained from model pastes, there was no formation of monosulfate in cement-slag A3 mixture even at 3 days. Also, reduced C−S−H gel phase and/or ettringite was noted in the real cement pastes, suggested by the reduced peak intensity at about 150 °C. It can be attributed to the slow hydration of C_2S and C_4AF in cement clinker.

XRD scans (Fig. 13 (a) and (c)) verified that monosulfate was detected in both model and real cement pastes of A12 and A18 at 3 days, in agreement with TGA results observed in Fig. 12. Ettringite persisted in all model blends at 3 days (in agreement with the conclusion obtained in Section 3.2.1), and the transformation from ettringite to monosulfate proceeded continuously with the increasing alumina content in slag. The peak of ettringite even vanished in cement-slag A18 paste. As for hydrotalcite-like phase, it was not clear at this stage, possibly owing to its poor crystallinity. The peak for C_3A was still distinct in C_3S-C_3A-5 % SO_3-slag A3 and A12 blends while it almost disappeared in the model paste of slag A18. As discussed above, the hydration of C_3A was enhanced with the 'activation' of slag, especially for that rich in alumina (Fig. 10). Also, C_3A was not detected in all cement-slag systems. It was reasonable as C_3A was only a minor component of cement clinker, rather than a pure agent blended with other raw materials in the model paste.

Table 3
Rate-controlling factor of aluminate reaction in each run of C_3S-C_3A-SO_3-slag systems.

	A3	A12	A18
G3	AlO_2^-	SO_4^{2-}	SO_4^{2-}
G5	AlO_2^-	SO_4^{2-}	SO_4^{2-}
G10	AlO_2^-	AlO_2^-	SO_4^{2-}

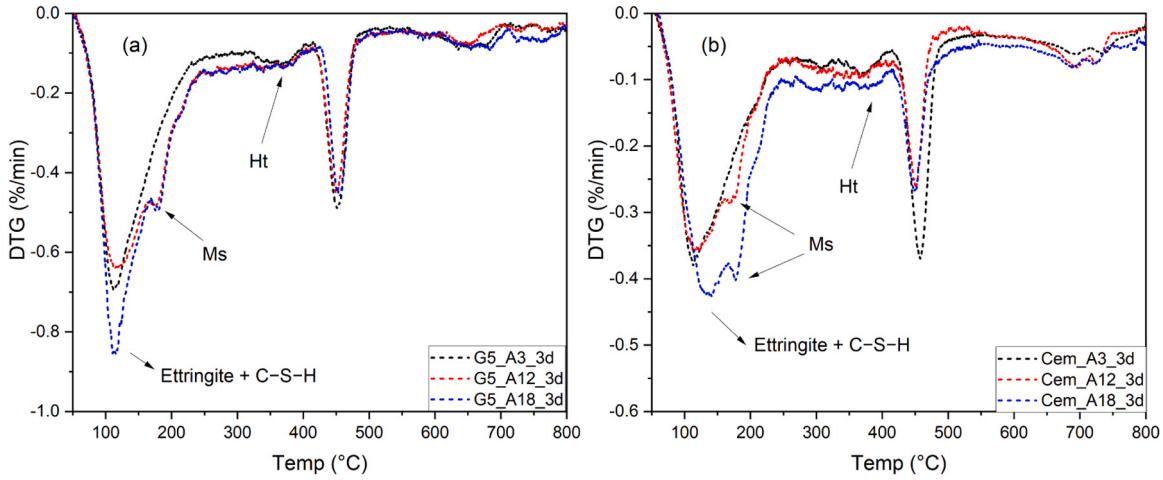

Fig. 12. Exemplary results of DTG analysis of (a) C_3S-C_3A-5 % SO_3-slag mixtures and (b) cement-slag mixtures after 3 days of curing. Ms: monosulfate; Ht: hydrotalcite-like phase.

When comparing C_3S-gypsum-slag system, the incorporation of C_3A modified the evolution of phase assemblage with time. C−S−H gel phase, portlandite, and ettringite were identified as the main hydration products of all systems studied at an early age. However, it should be noted that monosulfate was only visible in C_3S-gypsum-Al_2O_3-rich slag system (i.e., A18) while it was observed in both slag A12 and A18 pastes with the addition of C_3A, no matter in the form of pure agent in the model paste or as component of cement clinker in real blended paste.

3.4. Morphology of hydration products

Fig. 14 (a)-(c) illustrates the morphology of different hydrates formed in the model paste after 3 days of curing, using C_3S-C_3A-5 % SO_3-slag A12 blend as an example. Numerous long needle-like crystals implied the precipitation of ettringite, with a length of about several microns. Thin plates of portlandite can also be identified intermixed with ettringite (Fig. 14 (a)). Fibrillary C−S−H gel phase was clearly seen in Fig. 14 (b) and (c), exhibiting the morphology of blooming flowers with ettringite embedding. These results were consistent with thermal analysis present in Section 3.3 and in accordance with conclusions obtained in [36], which proved that the addition of gypsum modified the morphology of C−S−H gel phase into a divergent fibrillary-like phase by promoting repulsion among structures.

Fig. 14 (d) and (e) clearly show that different hydrates, e.g., C−S−H gel phase and ettringite, were precipitated on the surface of slag grains. Up to 3 days of curing when most C_3S had been hydrated, intact slag surface with large particle size can still be visualized ((d)-(f)). These observations emphasized that large slag grains hydrated slowly at this early age, and etch pits caused by the attack of OH^- ions were nearly invisible. Some isolated nucleis and/or clusters were anchored on the surface.

Compared to the morphology of hydrates formed in C_3S-5 % SO_3-slag A12 blend at 3 days (Fig. 15 in [19]), the incorporation of C_3A changed the morphology of ettringite considerably. The well crystallized ettringite observed in this work should be sourced from the reaction between C_3A and gypsum. However, in mixtures when without C_3A addition, only aluminate phase dissolved from slag took part in the formation of ettringite. Consequently, ettringite was relatively poorly organized and crystallized, despite still presenting a needle-like morphology.

4. Discussion

In this part, thermodynamic modelling based on GEMS was implemented, and the modelling and experimental results were compared and discussed qualitatively and quantitatively. Besides, equation with respect to the optimal gypsum addition was proposed.

4.1. Effect of C_3A addition and Al_2O_3 content of slag

Fig. 15 elaborates the influence of Al_2O_3 content in slag on the volume of phase assemblage, using C_3S-C_3A-5 % SO_3-slag system as an example. To simplify the simulation, the adopted hydration degree was 80 % for C_3S, 70 % for C_3A, 100 % for gypsum, and 15 % for slag at 3 days (Fig. 10). It was worthwhile to mention that the hydration degrees of C_3A and slag fluctuated when with different alumina contents in slag.

As observed, increasing alumina content firstly increased the amount of ettringite formed until the consumption of gypsum (circled as P in the graph). The volume of hydrates also went up slightly. At this stage, ettringite was stabilized in the system as gypsum was surplus. In other words, gypsum was abundant when slag only contained few alumina, and it was mainly consumed in the aluminate reaction with C_3A.

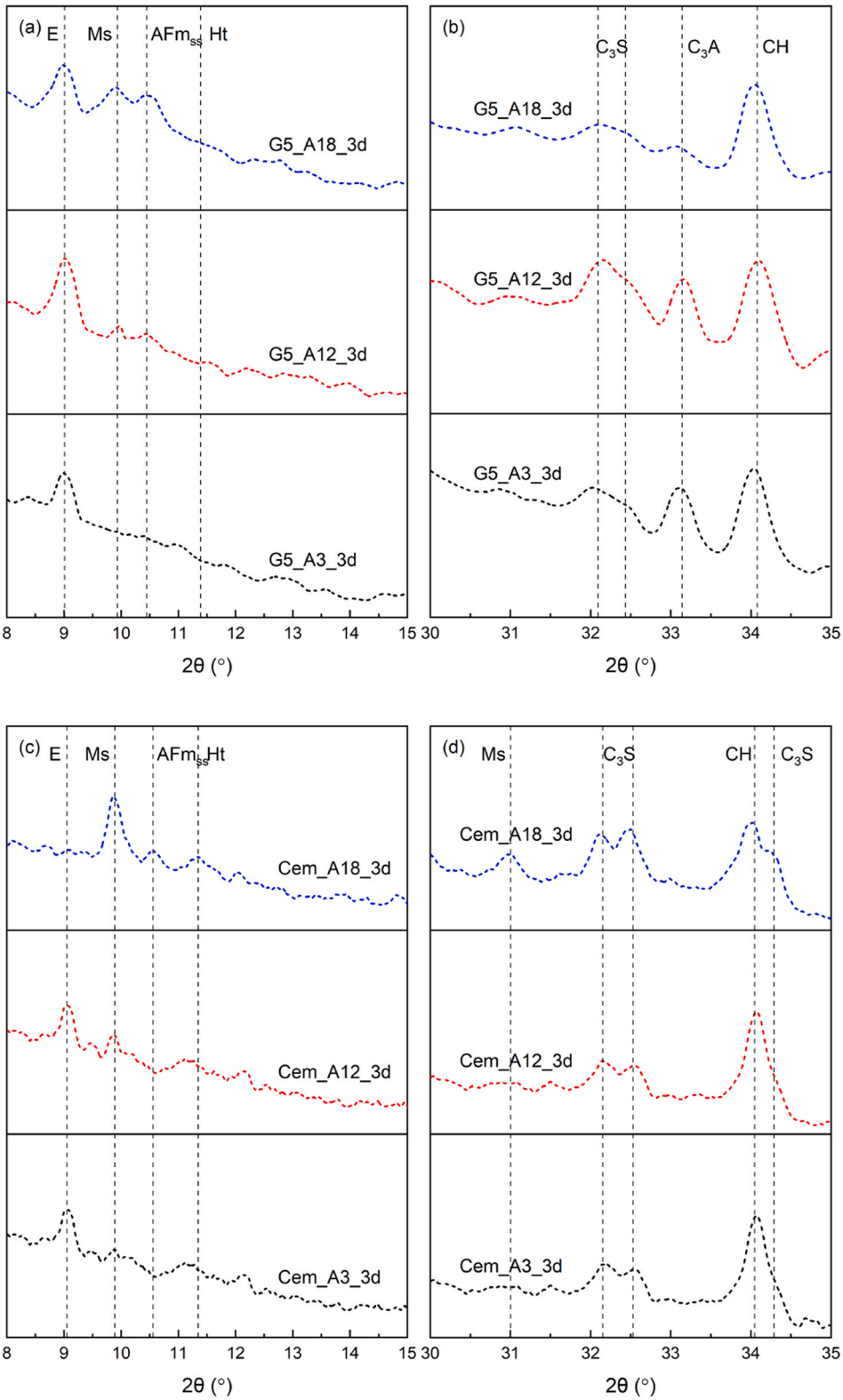

Fig. 13. XRD analysis of (a, b) C_3S-C_3A-5 % SO_3-slag mixtures and (c, d) cement-slag mixtures after 3 days of curing. CH: portlandite; E: ettringite; Ms: monosulfate; AFm_{ss}: solid solution of hemicarbonate and OH^- substituted monosulfate; Ht: hydrotalcite-like phase.

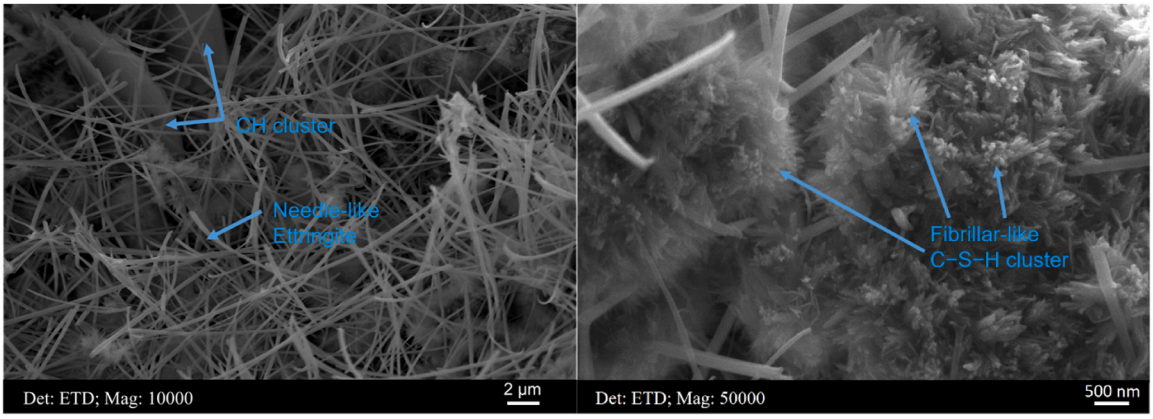

(a) morphology of portlandite and ettringite (b) morphology of fibrillar-like C−S−H gel phase

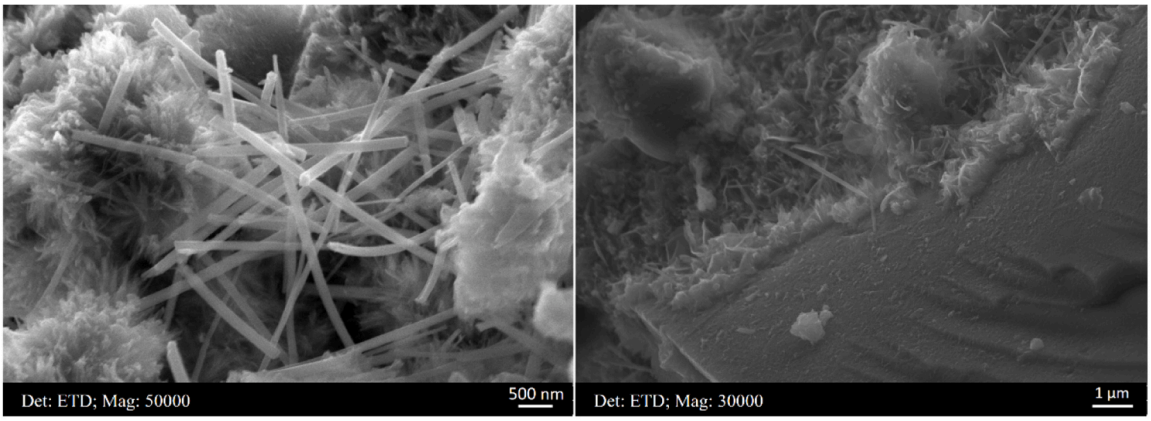

(c) morphology of fibrillar-like C−S−H gel phase (d) hydrates precipitated on the surface of slag grains

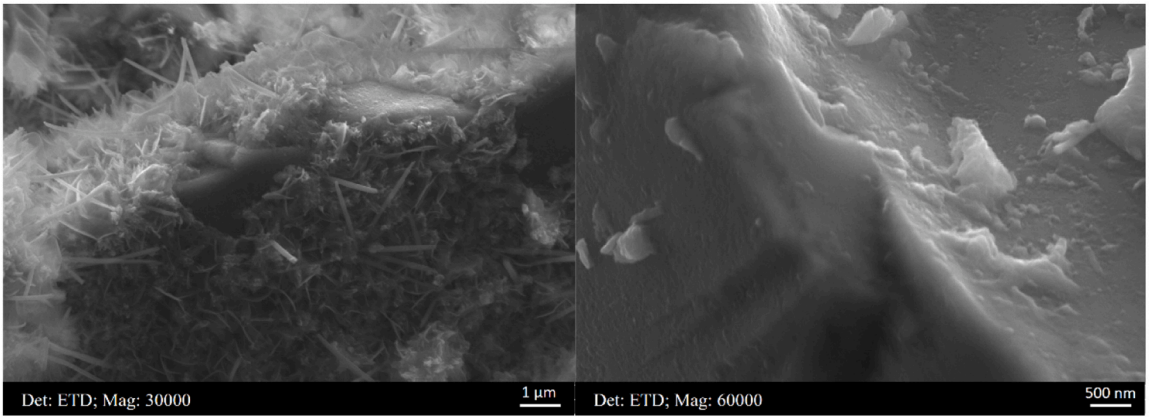

(e) hydrates precipitated on the surface of slag grains (f) intact slag surface

Fig. 14. Morphology of hydrates in C_3S-C_3A-5 % SO_3-slag A12 blend at 3 days.

Subsequently, the transformation from ettringite to monosulfate started. Slag A3 was just located around this inflection point (P), approximately. It was consistent with the results yielded by TGA (Fig. 12) and XRD (Fig. 13) that no monosulfate was detected in slag A3 blend at 3 days. With the further incorporation of Al_2O_3, the precipitation of monosulfate became increasingly prominent at the consumption of ettringite (slag A12 and A18 mixtures), also matched with the results measured through TGA and XRD. These results

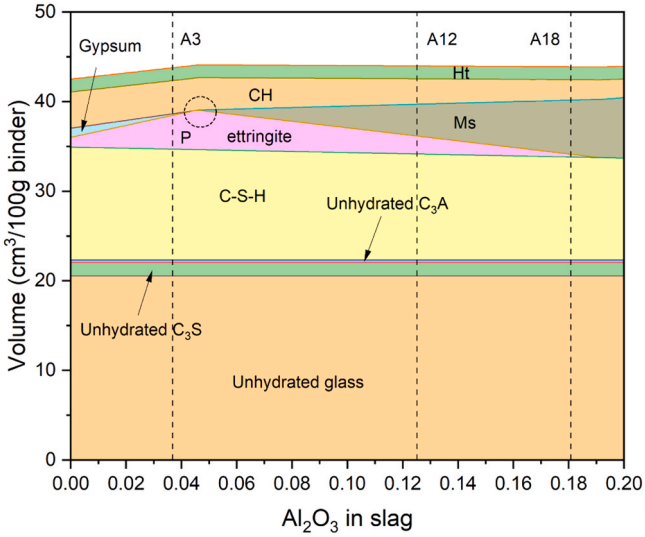

Fig. 15. Changes in the total volume of hydrates as an effect of Al_2O_3 content in slag after 3 days of hydration. The dash lines represent three synthetic slag levels that were investigated in the present study. C_3S-C_3A-5 % SO_3-slag system was considered here. Volume expressed as cm^3/100 g unhydrated binder. CH: portlandite; Ht: hydrotalcite-like phase; Ms: monosulfate.

verified the following formula regarding the precipitation of monosulfate, involving the participation of ettringite and aluminate species dissolved from slag. As for Ca^{2+} ion, it can be originated from portlandite and/or C−S−H gel phase, the volume of which both decreased gradually.

$$Ca_6Al_2(SO_4)_3(OH)_{12}\cdot 26H_2O + 6Ca^{2+} + 8OH^- + 4AlO_2^- \rightarrow 3Ca_4Al_2(SO_4)(OH)_{12}\cdot 6H_2O$$

Compared to C_3S-5 % SO_3-slag system (see Figure 17 in [19]), the introduction of C_3A did not modify the volume of total hydrates considerable. However, it accelerated the occurrence of monosulfate. It was expected as the dissolution of C_3A enhanced the concentration of aluminate phase in the pore solution, which can contribute to the formation of ettringite, as well as its transformation to monosulfate. On the other hand, it should be noted that owing to the limitation of this technique, the interaction among C_3A and slag (Section 3.2.4) cannot be realized in the modelling.

Overall, at 5 % sulfate dosage level (corresponding to 3.225 g gypsum/100 g binder), the effect of C_3A incorporation and variable Al_2O_3 contents in slag on hydrates volume at an early age was negligible. Although ettringite with a larger molar volume disappeared earlier with the C_3A introduction and gradual increase of Al_2O_3 in slag, the mass production of monosulfate can still fill up pores, thus being beneficial for the early-age compressive strength development [37].

4.2. *Effect of gypsum*

Fig. 16 (a) and (b) elaborate the influence of gypsum on the phase assemblage volume based on C_3S-C_3A-gypsum-slag A12 and A18 mixtures, respectively. The interaction between C_3A and slag, i.e., the suppression effect of C_3A on slag hydration and activation effect of alumina in slag on C_3A hydration were considered. The hydration degrees of C_3A and slag were assumed to be 60 % and 10 % in slag A12 blend as well as 70 % and 15 % for slag A18 paste, respectively. The hydration degree of C_3S was kept at 80 %.

When without gypsum incorporation, both mixtures can be considered as an undersulfated system, and aluminate species dissolved from C_3A and slag would participate into the formation of C_3AH_6 [28,38]. This phase vanished with the stepwise addition of gypsum, accompanied by the increasing generation of monosulfate and volume of total hydrates. It was suggested that aluminate phase was adequate at this stage and it prevented the precipitation of ettringite. When C_3AH_6 disappeared totally, the volume of phase assemblage reached the maximum (defined as ***optimal gypsum content*** in this study). With the continuous incorporation of gypsum, ettringite started to occur in the system. In slag A12 blend, gypsum became surplus when more than 6.0 g/(100 g binder) was added. As for slag A18 paste, no gypsum was left due to its high alumina content. Although the volume of ettringite increased remarkably with the increasing gypsum content, it just compensated the reduction of monosulfate and C−S−H gel phase. The total volume of hydrates exhibited minor fluctuation after the inflection point circled in the plots. Additionally, because of the higher hydration degree of reactants, more hydrates with larger volume were generated in C_3S-C_3A-gypsum-slag A18 mixture.

~1.6 g/(100 g binder) gypsum was determined to maximize the volume of phase assemblage of slag A12 paste after 3 days of hydration. This value was close to the gypsum content found in CEM I 42,5 N, which was ~1.9 g/(100 g binder) roughly based on Bouge calculation. As for Al_2O_3-rich slag system, e.g., slag A18, the optimal mass of gypsum rose to ~2.6 g/(100 g binder). This value was significantly higher than the gypsum content in cement. Thus, it was necessary to adjust the amount of gypsum manually.

With these results, it was possible to conclude that the optimal sulfate requirement of blended cement was strongly associated with

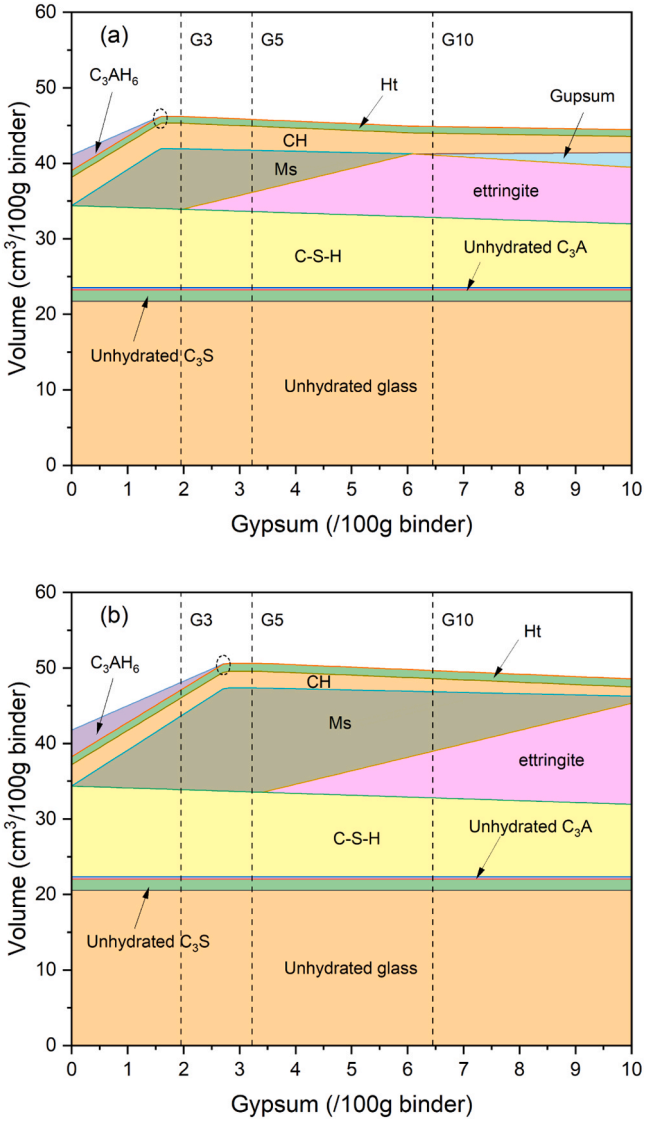

Fig. 16. Changes in the total volume of hydrates as an effect of gypsum for slag (a) A12 and (b) A18 mixtures. The chemical composition of slag A12 and A18 in Table 1 was adopted, respectively throughout the modelling. Volume expressed as cm^3/100 g unhydrated binder.

parameters, including C_3A content in cement clinker, slag substitution level, slag chemistry (Al_2O_3 and MgO), and hydration degree of slag, etc. For CEM III/B when C_3A hydrated almost completely at 3 days, slag chemistry and its hydration degree dominated. Slag chemistry affected its reactivity thus its hydration degree remarkably. In the present study, it was calculated that 15 % slag had been dissolved at 3 days in the model paste of A18, and this value reduced to 10 % and 7 % for slag A12 and A3 blends, respectively. It agreed well with the results found in [22,34,35] that slag reactivity exhibited a decreasing trend with reduced alumina content. Besides, it was already confirmed that most fine slag grains hydrated at an early age [39,40]. Thus, when ultra-fine slag particle was adopted in the mixture, e.g., for ultra-high-performance concrete, a higher slag hydration degree would be expected, more aluminate phase would be released by slag and enter the pore solution, and thus more gypsum was needed to achieve the maximal phase volume. On the contrary, MgO-rich slag can reduce the sulfate requirement of the blended system, by fixing aluminum into hydrotalcite-like phase with much lower solubility products [41].

Collectively, instead of using the same gypsum content in Ordinary Portland cement, the industry and academia should have a better understanding of alumina content in slag on sulfate requirement of cement-slag system, especially when high slag replacement level (e.g., 70 % employed in this study to simulate CEM III/B), Al_2O_3-rich slag (e.g., slag A18), and ultra-fine slag (e.g., for the production of ultra-high-performance concrete) are considered for the mixture. Optimal gypsum content can be obtained through above equation and/or thermodynamic modelling of the target mixture.

5. Conclusions

The present research investigated the hydration characteristics of model (C_3S-C_3A-gypsum-blast furnace slag) and real cement slag pastes at an early age, and emphasis was laid on the interaction of gypsum, aluminate phases dissolved from both C_3A and slag. To be compatible with the variation of alumina content of slag across different regions [13–15], synthetic slags with Al_2O_3 from 3.69 to 18.19 wt% were produced. The main conclusions were drawn as follows:

- With the incorporation of C_3A, two additional peaks arose during the decelerating stage of calorimetric measurement, both of which were delayed with the progressive addition of gypsum. The first peak was originated from the renewed aluminate reaction between C_3A and gypsum, while the second one was attributed to the reaction between sulfate and aluminate species dissolved from slag, which was less reactive compared to C_3A.
- High alumina content in slag promoted the aluminate reactions between gypsum and C_3A, and the hydration degree of C_3A exceeded 80 % at 10 % sulfate content. However, the reaction between slag and gypsum was suppressed because of the addition of C_3A, and the hydration degree of slag A18 was reduced to less than 10 %
- When without C_3A incorporation, monosulfate was only visible in Al_2O_3-rich slag paste (A18); however, it was detected in both A12 and A18 pastes with the incorporation of C_3A, in both model and real cement pastes.
- The optimal sulfate requirement was associated with parameters including C_3A content in cement clinker, slag substitution level, slag chemistry, and hydration degree of slag. Especially, it was increased with increasing alumina content in slag, reaching ~2.6 g/(100 g binder) for slag A18 blends.

CRediT authorship contribution statement

Yu Zhang: Writing – original draft, Methodology, Investigation, Conceptualization. **Chaoyu Liu:** Writing – review & editing, Investigation. **Luiz Miranda de Lima Junior:** Methodology. **Chen Liu:** Writing – review & editing, Supervision, Investigation.

Declaration of Competing Interest

The authors declare that they have no known competing financial interests or personal relationships that could have appeared to influence the work reported in this paper.

Acknowledgements

Start-up Research Fund of Southeast University (Grant Number RF1028623287) is gratefully acknowledged for the financial support.

Data availability

Data will be made available on request.

References

[1] Allen, M., M. Babiker, Y. Chen, et al. Global warming of 1.5 °C: An IPCC Special Report. (Accessed ⟨https://www.ipcc.ch/site/assets/uploads/sites/2/2022/06/SPM_version_report_LR.pdf⟩).
[2] K.H. Yang, Y.B. Jung, M.S. Ch, et al., Effect of supplementary cementitious materials on reduction of CO_2 emissions from concrete, J. Clean. Prod. 103 (15) (2015) 774–783.
[3] M. Juenger, R. Siddique, Recent advances in understanding the role of supplementary cementitious materials in concrete, Cem. Concr. Res. 78 (2015) 71–80.
[4] C. Liu, Z. Li, G. Ye, Mechanisms of efflorescence of alkali-activated slag, Cem. Concr. Compos. 155 (2025) 105811.
[5] M. Juenger, R. Snellings, S. Bernal, Supplementary cementitious materials: New sources, characterization, and performance insights, Cem. Concr. Res. 122 (2019) 257–273.
[6] R. Snellings, P. Suraneni, J. Skibsted, Future and emerging supplementary cementitious materials, Cem. Concr. Res. 171 (2023) 107199.
[7] P. Durdziński, R. Snellings, C. Dunant, et al., Fly ash as an assemblage of model Ca–Mg–Na-aluminosilicate glasses, Cem. Concr. Res. 78 (2015) 263–272.
[8] M. Antoni, J. Rossen, F. Martirena, et al., Cement substitution by a combination of metakaolin and limestone, Cem. Concr. Res. 42 (12) (2012) 1579–1589.
[9] Y. Yang, K. Raipala, L. Holappa, Ironmaking. Treatise on process metallurgy, Elsevier, 2014.
[10] I. Sohn, D. Min, A review of the relationship between viscosity and the structure of calcium-silicate-based slags in ironmaking, Steel Res. Int. 83 (7) (2012) 611–630.
[11] E. Crossin, The greenhouse gas implications of using ground granulated blast furnace slag as a cement substitute, J. Clean. Prod. 95 (15) (2015) 101–108.
[12] E. Özbay, M. Erdemir, H. Durmuş, Utilization and efficiency of ground granulated blast furnace slag on concrete properties-A review, Constr. Build. Mater. 105 (15) (2016) 423–434.
[13] Granulated Blastfurnace Slag. Technical Leaflet No. 1. (Accessed by ⟨https://www.euroslag.com/wp-content/uploads/2018/12/LeafletGBS.pdf⟩).
[14] ACI Committee 233 Report. Slag Cement in Concrete and Mortar. 2003. (Accessed by ⟨http://civilwares.free.fr/ACI/MCP04/233R_03.PDF⟩).
[15] 20 ×10 mm Concrete Aggregate. Technical Leaflet No. 1. (Accessed by ⟨http://www.asms.com.au/applications/20x10mm-concrete-aggregate⟩).
[16] J. Bijen, Benefits of slag and fly ash, Constr. Build. Mater. 10 (5) (1996) 309–314.
[17] S. Nie, R.M. Thomsen, J. Skibsted, Impact of Mg substitution on the structure and pozzolanic reactivity of calcium aluminosilicate (CaO-Al_2O_3-SiO_2) glasses, Cem. Concr. Res. 138 (2020) 106231.
[18] A. Hamdan, A. Hajimohammadi, B. Njegic, et al., The changes in the reaction kinetics and phase assemblage of sodium silicate-activated CaO-MgO-Al_2O_3-SiO_2 glasses induced by the Al replacement by Mg, Cem. Concr. Res. 166 (2023) 107103.

[19] Y. Zhang, Z. Wan, L. de Lima Junior, et al., Early age hydration of model slag cement: Interaction among C_3S, gypsum and slag with different Al_2O_3 contents, Cem. Concr. Res. 161 (2022) 106954.
[20] F. Zunino, K. Scrivener, Factors influencing the sulfate balance in pure phase C_3S/C_3A systems, Cem. Concr. Res. 133 (2020) 106085.
[21] S. Joseph, J. Skibsted, Ö. Cizer, A quantitative study of the C_3A hydration, Cem. Concr. Res. 115 (2019) 145–159.
[22] Y. Zhang, S. Zhang, Y. Chen, et al., The effect of slag chemistry on the reactivity of synthetic and commercial slags, Constr. Build. Mater. 335 (2022) 127493.
[23] K. Shimoda, Y. Tobu, K. Kanehashi, et al., Total understanding of the local structures of an amorphous slag: perspective from multi-nuclear (^{29}Si, ^{27}Al, ^{17}O, ^{25}Mg, and ^{43}Ca) solid-state NMR, J. NonCryst. Solids 354 (10-11) (2008) 1036–1043.
[24] T. Wagner, D. Kulik, F. Hingerl, et al., GEM-Selektor geochemical modeling package: TSolMod library and data interface for multicomponent phase models, Can. Mineral. 50 (5) (2012) 1173–1195.
[25] D. Kulik, T. Wagner, S. Dmytrieva, et al., GEM-Selektor geochemical modeling package: revised algorithm and GEMS3K numerical kernel for coupled simulation codes, Comput. Geosci. 17 (2013) 1–24.
[26] T. Matschei, B. Lothenbach, F. Glasser, Thermodynamic properties of Portland cement hydrates in the system $CaO-Al_2O_3-SiO_2-CaSO_4-CaCO_3-H_2O$, Cem. Concr. Res. 37 (10) (2007) 1379–1410.
[27] M. Whittaker, M. Zajac, M. Haha, et al., The role of the alumina content of slag, plus the presence of additional sulfate on the hydration and microstructure of Portland cement-slag blends, Cem. Concr. Res. 66 (2014) 91–101.
[28] A. Quennoz, K. Scrivener, Interactions between alite and C_3A-gypsum hydrations in model cements, Cem. Concr. Res. 44 (2013) 46–54.
[29] J. Neto, E. Rodríguez, P. Monteiro, et al., Hydration of C_3S and Al-doped C_3S in the presence of gypsum, Cem. Concr. Res. 152 (2022) 106686.
[30] H. Minard, S. Garrault, L. Regnaud, et al., Mechanisms and parameters controlling the tricalcium aluminate reactivity in the presence of gypsum, Cem. Concr. Res. 37 (10) (2007) 1418–1426.
[31] J. Bullard, H. Jennings, R. Livingston, et al., Mechanisms of cement hydration, Cem. Concr. Res. 41 (12) (2011) 1208–1223.
[32] K. Scrivener, R. Snellings, B. Lothenbach, A practical guide to microstructural analysis of cementitious materials, CRC Press, 2018.
[33] E. Berodier, Impact of the supplementary cementitious materials on the kinetics and microstructural development of cement hydration, EPFL, 2015.
[34] S. Kucharczyk, M. Zajac, C. Stabler, et al., Structure and reactivity of synthetic $CaO-Al_2O_3-SiO_2$ glasses, Cem. Concr. Res. 120 (2019) 77–91.
[35] S. Blotevogel, A. Ehrenberg, L. Steger, et al., Ability of the R3 test to evaluate differences in early age reactivity of 16 industrial ground granulated blast furnace slags (GGBS), Cem. Concr. Res. 130 (2020) 105998.
[36] B. Mota, T. Matschei, K. Scrivener, The influence of sodium salts and gypsum on alite hydration, Cem. Concr. Res. 75 (2015) 53–65.
[37] P. Termkhajornkit, Q. Vu, R. Barbarulo, et al., Dependence of compressive strength on phase assemblage in cement pastes: Beyond gel-space ratio-Experimental evidence and micromechanical modeling, Cem. Concr. Res. 56 (2014) 1–11.
[38] J. Plank, Z. Dai, H. Keller, et al., Fundamental mechanisms for polycarboxylate intercalation into C_3A hydrate phases and the role of sulfate present in cement, Cem. Concr. Res. 40 (1) (2010) 45–57.
[39] Y. Zhang, X. Zhang, Grey correlation analysis between strength of slag cement and particle fractions of slag powder, Cem. Concr. Compos. 29 (6) (2007) 498–504.
[40] P. Wang, R. Trettin, V. Rudert, Effect of fineness and particle size distribution of granulated blast-furnace slag on the hydraulic reactivity in cement systems, Adv. Cem. Res. 17 (4) (2005) 161–167.
[41] R. Myers, B. Lothenbach, S. Bernal, et al., Thermodynamic modelling of alkali-activated slag cements, Appl. Geochem. 61 (2015) 233–247.